

Liver Segment Approximation in CT Data for Surgical Resection Planning

Reinhard Beichel^a, Thomas Pock^a, Christian Janko^a, Roman Zotter^a, Bernhard Reiteringer^a, Alexander Bornik^a, Kálmán Palágyi^b, Erich Sorantin^c, Georg Werkgartner^d, Horst Bischof^a, and Milan Sonka^e

^aInstitute for Computer Graphics and Vision, Graz University of Technology, Inffeldgasse 16, A-8010 Graz, Austria;

^bDept. of Image Processing and Computer Graphics, University of Szeged, Árpád tér 2, H-6720 Szeged, Hungary;

^cDept. of Radiology, University Hospital Graz, Auenbruggerplatz 9, A-8036 Graz, Austria;

^dDept. of Surgery, University Hospital Graz, Auenbruggerplatz 29, A-8036 Graz, Austria;

^eDept. of ECE, The University of Iowa, Iowa City, IA 52242, USA

ABSTRACT

Surgical planning of liver tumor resections requires detailed three-dimensional (3D) understanding of the complex arrangement of vasculature, liver segments and tumors. Knowledge about location and sizes of liver segments is important for choosing an optimal surgical resection approach and predicting postoperative residual liver capacity. The aim of this work is to facilitate such surgical planning process by developing a robust method for portal vein tree segmentation. The work also investigates the impact of vessel segmentation on the approximation of liver segment volumes. For segment approximation, smaller portal vein branches are of importance. Small branches, however, are difficult to segment due to noise and partial volume effects. Our vessel segmentation is based on the original gray-values and on the result of a vessel enhancement filter. Validation of the developed portal vein segmentation method in computer generated phantoms shows that, compared to a conventional approach, more vessel branches can be segmented. Experiments with in vivo acquired liver CT data sets confirmed this result. The outcome of a Nearest Neighbor liver segment approximation method applied to phantom data demonstrates, that the proposed vessel segmentation approach translates into a more accurate segment partitioning.

Keywords: Vessel segmentation, liver segment approximation, liver resection planning

1. INTRODUCTION

Optimal surgical treatment of patients suffering from liver tumors depends on exact anatomical information regarding the involved liver segments and vascular anatomy. This is especially the case for liver resections, where a decision has to be made, whether a liver-segment-based or an atypical resection should be carried out.¹ Therefore, volumetry of the whole organ and of the individual liver segments is mandatory, in order to estimate postoperative residual liver capacity.

Imaging modalities like Computed Tomography (CT) do not allow a noninvasive direct visualization of the individual liver segments. Segment boundaries can only be approximated by the corresponding liver vessels. The partitioning scheme proposed by Couinaud² evolved as a standard,³ where three planes and transverse scissura are arranged according to the main portal and hepatic vein branches to classify eight (autonomous) liver segments. An application of Couinaud's scheme to the planning of liver resections based on CT volume data is quite demanding, since physicians have to mentally deal with the segment partitioning and additionally consider liver tumors and vasculature. Several approaches to computer aided liver surgery planning have been developed in the last years, in order to ease this process.⁴⁻¹¹

Further author information: (Send correspondence to R.B.)

R.B.: E-mail: beichel@icg.tu-graz.ac.at, Telephone: +43 (316) 873 5022, WWW: <http://liverplanner.icg.tu-graz.ac.at>

As reported in,^{3,12,13} Couinaud-based liver segment partitioning has some limitations. It can be regarded as a rough anatomic classification scheme. In practice, differences between preoperative assessments and interoperative findings occur frequently. Therefore, most of the liver surgery planning systems developed to date apply approximation methods, that are similar to Couinaud’s scheme, but adapt more flexible regarding the patient specific vascular topology (see Section 1.2). However, an investigation of computer aided segment approximation methods published in¹⁴ shows, that the number of portal vein branching generations segmented has an influence on: (A) the accuracy of the segment approximation and (B) the selection of the optimal approximation method.

1.1. Vessel segmentation and skeletonization methods

Clearly, portal vein segmentation is a critical part of the success and quality of an automated segment approximation. Issues like inhomogeneous low contrast vessels, inhomogeneous liver tissue appearance or contrast enhanced tumors that might cause leakage have to be considered. Several methods for liver vessel segmentation in CT data have been reported.^{6,8,9,14} For example, a refined region growing algorithm, which automatically suggests a threshold to be used as a stopping criterion, was proposed in.¹⁴ The algorithm allows manual intervention regarding the threshold selection.

More generally, multi-scale analysis of tubular structures based on normalized second derivatives and the eigenvalues/eigenvectors of the Hessian matrix has been proposed for applications like 3D vessel enhancement¹⁵ and segmentation.¹⁶ By using the Hessian, discrimination between tubular and other structures like sheets or blobs is possible, which improves results in low contrast cases or when a non-tubular object with a similar gray-value is adjacent. This approach has been successfully applied to several tubular structure analysis tasks, as documented by several publications.^{17–26} Multi-scale line analysis has also been used in the context of liver vasculature analysis. An algorithm for the centerline extraction of tubular objects was reported in²³ and applied to liver CT and liver 3D ultrasound as well as to other data sets. Several heuristics are proposed to improve the tracking procedure, in order to recover from local discontinuities and to avoid other problems. In¹⁷ a multi-scale line filter was proposed for the segmentation and visualization tasks and applied to the contrast dye enhanced portal vein vessels. For segmentation the original and vessel enhanced volume data were thresholded and smaller disconnected objects were removed. Visual comparison by using a surface rendering technique showed, that a larger percentage of smaller vessels was segmented in the line filtered volume without leaking into surrounding liver tissue.

Depending on the used scanning protocol and on data quality, it might be necessary to separate the portal vein from other liver vessel systems (e.g.: hepatic veins) after segmentation. For this task, several automated and interactive approaches have been reported by using skeletonization, branch–point identification and vessel diameter calculation methods.^{6,8,14} A skeleton is a frequently applied shape feature to represent the general form of an object. There are three major skeletonization techniques: distance–based (i.e., ridge extraction from the distance map of the boundary), Voronoi–based (i.e., extracting skeletal elements from the Voronoi diagram of the sampled boundary), and thinning (i.e., iterative object reduction).²⁷ A skeletonization method that can suppress the creation of unwanted skeleton surface patches was proposed in,^{28,29} where a 3D curve–thinning algorithm was used, that is capable of extracting 1–voxel wide centerlines.

1.2. Approximation of liver segments

Liver segments cannot be seen directly in CT image data. However, each segment can be defined by the topology of its own autonomous portal vessel supply tree. The main limitation of this approach is that the resolution of CT systems in current clinical use allow only to track the portal veins up to about the fourth branching level.³⁰ Therefore, the information about the eight liver segments cannot be directly reconstructed from the obtained portal vein tree. The lack of information forces an approximation of the segments based on the supplying vessel topology. Basically, this task can be seen as a classification problem.

Work on segment approximation reported in¹⁴ and in other publications of the same group has led to a nearest neighbor approximation (NNA) and a Laplacian approximation (LA) approach. The NNA assigns voxels to segments with the lowest Euclidean distance according to its defining portal branches. LA uses a metric derived from potential functions and is based on Laplacian equations.¹⁴ A voxel is assigned to a branch which yields the highest potential at its voxel position. Depending on the boundary conditions used, a basic and an

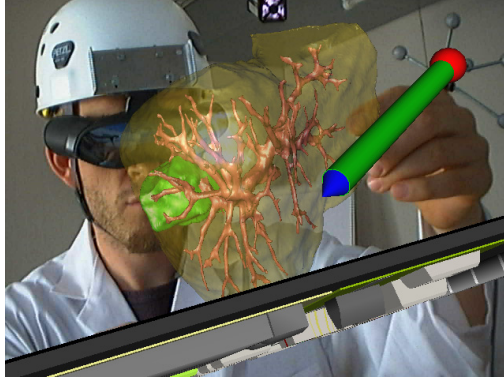


Figure 1. Augmented Reality (AR) based liver surgery planning in action.

extended version of the LA have been developed. The extended version additionally considers draining hepatic veins and the diameter of portal veins. Segment feeding vessels were identified automatically. Both methods are validated based on corrosion casts of human livers, showing that the extended LA method delivers better results than the normal LA and that the NNA outperforms the extended LA method, when applied to a portal vein tree with more branch generations segmented. Other approaches to liver segment approximation were reported in.^{6, 8, 13}

1.3. Overview

The aim of this work is to facilitate accurate liver segment approximation by developing a robust method for portal vein tree segmentation in CT data and to investigate the impact of vessel segmentation on the approximation of liver segment volumes. The proposed vessel segmentation takes special care of smaller low contrast vessel by using a “vessel mining” approach, because of their importance for the quality of the liver segment approximation.¹⁴ The idea behind “vessel mining” is the following: first identify all potential tubular structures in the search volume and then reconnect the found tube structures based on defined criteria like for example gray-value evidence. In this way leakage into other structures can be avoided and a higher robustness in cases with noise or anisotropic voxel sizes can be achieved, compared to simpler methods like region growing.

The approach to liver segment partitioning outlined in this paper has been developed for an Augmented Reality (AR) based virtual liver surgery planning system described in,^{10, 11} where tracked input devices and see-through head mounted displays are used to interact with patient data in three-dimensions (3D) to plan a liver resection (see Fig. 1).

2. METHODOLOGY

The proposed process of hepatic segment approximation in CT data consists of the following main processing steps: robust portal vein segmentation, formal tree representation generation, labeling of segment feeding vessels and segment approximation. In our case, only portal veins are considered for the partitioning. Therefore, contrast enhanced CT data sets depicting the vascular system in the portal phase are required as input. Additionally, it is assumed that a liver mask is provided.

2.1. Portal vein segmentation – “vessel mining”

The main objective for the segmentation step is to extract not only the main portal vessel tree, but also smaller more peripheral vessel branches. Clearly, the scanning protocol and data quality impose certain limits and have to be considered also for optimization of the whole process. The individual processing stages of the developed portal vein segmentation method are outlined in the following sections, where a vector $\mathbf{v} = (x, y, z)^T$ is used to describe a voxel by its spatial coordinates in x , y and z directions.

A) Preprocessing: Two preprocessing steps are performed. First, a gray-value transformation is applied, where the gray-value $I(\mathbf{v})$ of each voxel \mathbf{v} inside the liver mask L is transformed according to

$$\tilde{I}(\mathbf{v}) = \begin{cases} \frac{I(\mathbf{v}) - g_{low}}{g_{high} - g_{low}} & \text{if } g_{low} < I(\mathbf{v}) < g_{high} \\ 1 & \text{if } g_{high} \leq I(\mathbf{v}) \\ 0 & \text{else} \end{cases} \quad (1)$$

into a range between zero and one, whereas all voxels outside the liver mask L are set to zero. The gray-value range of interest is defined by g_{low} and g_{high} . Usually, the parameters have to be selected only once for a given scanning protocol. Second, anisotropic voxels are converted to isotropic voxels by using a sinc interpolation, if necessary.

B) Vessel enhancement: A multi-scale analysis of tubular structures is applied, in order to enhance vessels and therefore avoid leakage of the segmentation algorithm into non vessel structures (e.g. liver tissue) in low contrast or high noise cases. The enhancement step is based on the Hessian matrix

$$\mathcal{H}(\mathbf{v}) = \nabla^2 \tilde{I}(\mathbf{v}) = \begin{bmatrix} \tilde{I}_{xx}(\mathbf{v}) & \tilde{I}_{xy}(\mathbf{v}) & \tilde{I}_{xz}(\mathbf{v}) \\ \tilde{I}_{yx}(\mathbf{v}) & \tilde{I}_{yy}(\mathbf{v}) & \tilde{I}_{yz}(\mathbf{v}) \\ \tilde{I}_{zx}(\mathbf{v}) & \tilde{I}_{zy}(\mathbf{v}) & \tilde{I}_{zz}(\mathbf{v}) \end{bmatrix}, \quad (2)$$

which is used for the analysis of the local structure around the voxel \mathbf{v} in the volume data. To take different vessel diameters into account, several scale dependent Hessian matrices are calculated. This is done by using the second partial derivatives of a Gaussian kernel $G(\mathbf{v}, \sigma) = e^{-\|\mathbf{v}\|^2/[2\sigma^2]}/[sqrt(2\pi\sigma^2)]^3$ with different values of σ as approximation of the second derivatives of the Hessian $\mathcal{H}_\sigma(\mathbf{v})$ at scale σ :

$$\tilde{I}_{kl} = \frac{\partial^2 G(v, \sigma)}{\partial k \partial l} * \tilde{I}(\mathbf{v}). \quad (3)$$

Let λ_1 , λ_2 and λ_3 be the eigenvalues of the Hessian matrix $\mathcal{H}(\mathbf{v})$ ordered such that $\lambda_1 \geq \lambda_2 \geq \lambda_3$, and the corresponding eigenvectors \mathbf{e}_1 , \mathbf{e}_2 and \mathbf{e}_3 . The eigenvalues of the Hessian matrix can be used to distinguish between vessels and other structures. In the following an assessment scheme proposed in¹⁷ is used for this purpose. At a given scale σ , the Hessian matrix $\mathcal{H}(\mathbf{v}, \sigma)$ is calculated and a vessel (line) measure is defined as

$$\lambda_{123} = \begin{cases} |\lambda_3| \left(\frac{\lambda_2}{\lambda_3}\right)^{\gamma_{23}} \left(1 + \frac{\lambda_1}{|\lambda_2|}\right)^{\gamma_{12}} & \text{if } \lambda_3 < \lambda_2 < \lambda_1 \leq 0 \\ |\lambda_3| \left(\frac{\lambda_2}{\lambda_3}\right)^{\gamma_{23}} \left(1 - \alpha \frac{\lambda_1}{|\lambda_2|}\right)^{\gamma_{12}} & \text{if } \lambda_3 < \lambda_2 < 0 < \lambda_1 < \frac{|\lambda_2|}{\alpha} \\ 0 & \text{else} \end{cases} \quad (4)$$

Measures from different scales σ are combined to one response by evaluating

$$M(\mathbf{v}) = \max_{\sigma} R(\mathbf{v}, \sigma), \quad (5)$$

with $R(v, \sigma) = \sigma^2 \lambda_{123}(\sigma)$, whereas the term σ^2 is used to normalize the responses at different scales. $M(\mathbf{v})$ is calculated for all voxels \mathbf{v} with corresponding gray-values $\tilde{I}(\mathbf{v}) > 0$ and is directly used as measure for vesselness.

C) Segmentation: A two stage algorithm is used, which first finds a rough threshold, followed by an iterative region growing process. The algorithm is derived from a segmentation method for retinal vessels proposed in.²⁰ To roughly separate the enhanced vessels from the background, the Otsu algorithm³¹ is applied, which determines a threshold t_o that maximizes the between-class variance. Based on t_o , the volume is partitioned into background voxels $V_{bg} = \{v \in L | M(\mathbf{v}) \leq t_o\}$ and vessel voxels $V_{ve} = \{v \in L | M(\mathbf{v}) > t_o\}$. For each of the classes mean values (μ_{bg} , μ_{ve}) and standard deviations (σ_{bg} , σ_{ve}) are calculated. At the beginning of the iterative region growing, seed voxels are defined as follows: $S_{bg} = \{v \in L | M(\mathbf{v}) \leq \min\{\mu_{bg} + \sigma_{bg}, t_o\}\}$ for the background and $S_{ve} = \{v \in L | M(\mathbf{v}) \leq \max\{\mu_{ve} - \sigma_{ve}, t_o\}\}$ for the vessels. Only unlabeled voxels in a 26-connected neighborhood are considered during the growing process. The two classes are grown

simultaneously. Homogeneity criteria are defined for the background as $M(\mathbf{v}) \leq (1 + c_i)t_o$ and for vessels as $M(\mathbf{v}) \geq (1 - c_i)t_o$. The first iteration step starts with $c_1 = 0$. Homogeneity criteria are then successively relaxed by using $c_{i+1} = c_i + \beta$, where β is a fixed defined constant. The iteration stops, when no new voxels are labeled in an iteration step.

D) Reconnection of vessels: At branching points of vessels, vesselness values (Equation 5) are lower than the values obtained at “normal” vessels, since the assumption of a tube like structure is violated. In addition, other influences like noise and partial volume effects can lead to a similar situation. Parameters in Equation 4 could be chosen to abate these effects, but at the same time selectivity regarding tube structures will also be lowered. In order to tackle this problem, a reconnection algorithm, based on gray-value evidence is applied. In a first step, a 3D connected component labeling using a 26-connectivity is performed. Components with a voxel count lower than a threshold T_1 are removed, to avoid chaining effects based on CT noise induced responses. Then, starting from a manually identified root voxel of the main portal vein trunk, the minimum cost path reconnection process is started, which is described in the following. The process is restricted to components within a distance smaller than T_2 from the main trunk part. Costs between two voxels \mathbf{v}_i and \mathbf{v}_j are defined as follows:

$$W(i, j) = \begin{cases} \delta[\tilde{I}(\mathbf{v}_i)^{-1} + \tilde{I}(\mathbf{v}_j)^{-1}] & \text{if } \mathbf{v}_i \text{ and } \mathbf{v}_j \text{ are in a 26-connected neighborhood} \\ \infty & \text{else} \end{cases}, \quad (6)$$

where δ is the Euclidean distance between the neighboring voxels. The minimum cost path is calculated by using Dijkstra’s algorithm. A reconnection is only carried out, if the minimum costs are lower than a threshold T_3 . The gap between the two components is closed by using a locally restricted morphological closing operation. As for preprocessing, parameters are usually only chosen once for a given scanning protocol or voxel size, respectively. Optionally, to deal with breathing artifacts or other similar disturbances, the reconnection process can be applied recursively, starting with largest structure not connected so far.

Depending on the chosen selectivity of the vessel enhancement step (Section 2.1.B), it might occur that false non vessel objects can get connected to the main vessel tree. This case can be fixed manually by using an AR tool similar to that described in Section 2.3: first the object is selected in 3D and then deleted.

2.2. Formal tree representation generation

So far, the portal vein tree has been segmented and is represented as a binary voxel-level object in a volume data set. For the labeling of segment feeding branches, a formal tree representation is needed. Several processing steps are necessary for this conversion: tree root identification, skeletonization, pruning, identification of branch-points, and finally the generation of a formal tree structure. For the tasks described above, we use a method that was originally developed and validated for human airway tree analysis.^{28,29} In addition, the segmented portal tree is divided into branches by the same method, which are stored in a labeled volume data set, later needed for the liver segment approximation (see Section 2.4). The individual processing steps are described in more detail below:

- A) Identification of the tree root:** The manually selected root voxel acts as an anchor point during the centerline extraction (i.e., it cannot be deleted by the forthcoming iterative peeling process).
- B) Extraction of the 3D centerlines — skeletonization:** A sequential 3D curve-thinning algorithm was developed for extracting both geometrically and topologically correct centerlines. One iteration step of the object reduction process is decomposed into six successive sub-iterations according to the six main directions in 3D. Each sub-iteration consists of two phases; at first the border points according to the actual deletion direction that are simple (i.e., their deletion does not alter the topology of the image³²) and not line-end points are marked as potential deletable. Then marked points are checked: a marked point is deleted if it remains simple and is not a line-end point after the deletion of some previously visited marked points.

- C) Pruning:** Our centerline pruning uses both the branch length and the distance-from-surface (depth) information for the identification of the following pruning candidate: all branches are deleted if their lengths are shorter than a given threshold t_l and their associated branch-points are not closer to the border/surface of the elongated tree than a given threshold t_d . The pruning process can be repeated for different pairs of thresholds (t_l, t_d) . In our experience, 2 to 4 iterations typically provide satisfactory results.
- D) Identification of branch-points:** In a centerline, three types of points can be identified: endpoints (which have only one 26-neighbor³²), line-points (which have exactly two 26-neighbors), and branch-points (which have more than two 26-neighbors) that form junctions (bifurcations, trifurcations, etc.).
- E) Generation of a formal tree structure:** The centerlines are converted into a graph structure (each voxel corresponds to a graph node and there is an edge between two nodes if the corresponding voxels are adjacent). A similar structure is assigned to the branch-points. In the branch-tree, a path between two branch- or endpoints is replaced by a single edge.
- F) Tree partitioning:** The aim of the partitioning procedure is to partition all voxels of the tree into branches — each voxel is assigned a branch-specific label. There are two inputs for this process — the segmented binary volume and the formal tree structure corresponding to the centerlines. The output is a gray-level volume, in which value “0” corresponds to the background and different non-zero values are assigned to the voxels belonging to different tree branches/partitions.

2.3. AR based labeling of segment feeding portal vessels and vessel system separation

The selection of segment feeding vessels is done manually by using an Augmented Reality environment utilized for the overall surgical planning procedure,^{10,11} since tumors can lead to pathological changes in the vessel structure. The branch labeled voxels and the formal tree structure are used as input (see Section 2.2). The vessel tree is visualized in 3D and physicians are using a tracked pen to label the segment branches in a “point and click” fashion.³³ In the same way, a “stop label” can be set, to separate different vessel systems, if needed.

2.4. Liver segment approximation

Liver segment approximation can be seen as a classification problem, where a set of liver tissue voxels $P \subset L$ is classified into subsets $\{S_1, \dots, S_n\}$, representing the n liver segments. The number of segments and the corresponding segment feeding branches V_1, \dots, V_n are specified via the labeling step described in Section 2.3. In the following, a basic Nearest Neighbor approximation (NNA) method is described, which was originally proposed in.¹⁴ For classification of a liver tissue voxel \mathbf{v} , the minimal distances $D_i(\mathbf{v}) = \min_{\mathbf{v}_j \in V_i} \{\delta(\mathbf{v}, \mathbf{v}_j)\}$ to voxels of all segment vessel branches V_i with $i = 1, \dots, n$ are calculated, where δ denotes the Euclidean distance between two voxels. Based on these distances, a classification function Θ is defined as follows:

$$\Theta_{NNA}(\mathbf{v}) = j \quad \text{if} \quad D_j(\mathbf{v}) = \min_{i=1, \dots, n} \{D_i(\mathbf{v})\} \quad , \quad (7)$$

assigning a liver segment label according to the label of the closest segment defining vessel tree. This process is repeated for all voxels $v \in P$. Finally, all voxels with the same labels are assigned to the corresponding subsets $\{S_1, \dots, S_n\}$. Segments supplied by more than one branch from the main portal trunk are taken into account by splitting them and temporarily introducing new segments. After the intrinsic partitioning described above, this kind of liver subsegments are merged again to form one corresponding segment.

3. EXPERIMENTAL METHODS

3.1. Data

For validation of the segment approximation, a portal vein corrosion cast of a human liver (see Fig. 2.a) was CT scanned (LightSpeed QX/i, GE Medical Systems), with a voxel size of $0.53 \times 0.53 \times 0.5 \text{ mm}^3$ and a volume size of $512 \times 512 \times 465$ voxels. After the conversion of the CT scanned portal tree into a binary data set, the liver surface was reconstructed by using morphological operations, a simplex mesh,³⁴ and a voxelization method.³⁵ Reconstructing the exact original liver borders is not important in this case, since only the partitioning behavior

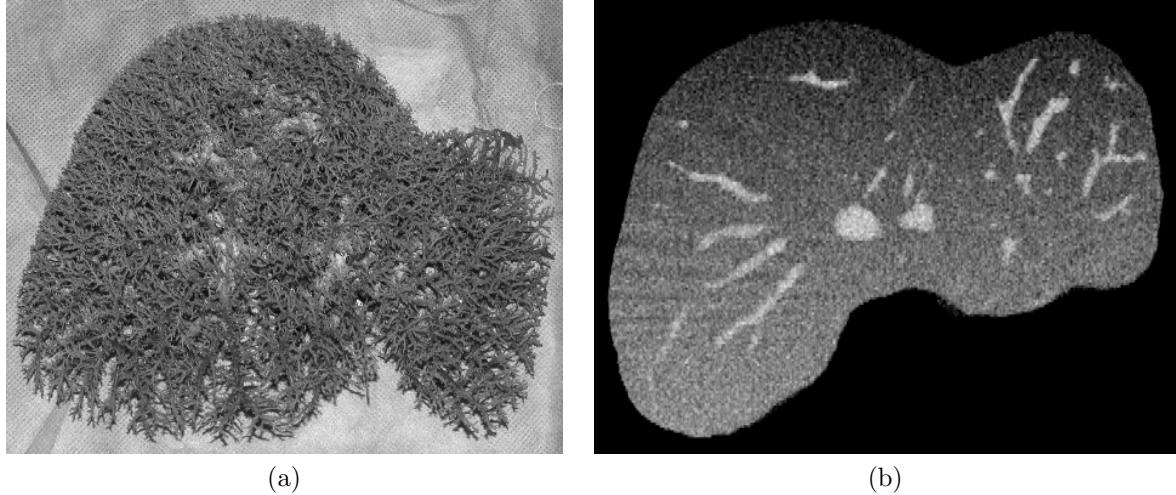


Figure 2. Data used for validation. (a) Liver portal vein corrosion cast. (b) Phantom liver data set based on the scanned corrosion cast.

of the segment approximation is of interest. The vessel tree of the corrosion cast shows a large number of branches, compared to portal trees extracted from conventional in vivo CT scans. For validation purposes, a pruned version of the segment portal vein cast was generated (later called reference segmentation) to simulate normal examination conditions. Segment feeding tree branches of the pruned version were labeled by using an AR based tool (see Section 2.3) and liver segments were approximated by using the NNA method (see Section 2.4). The obtained segment approximation was then utilized as a reference.

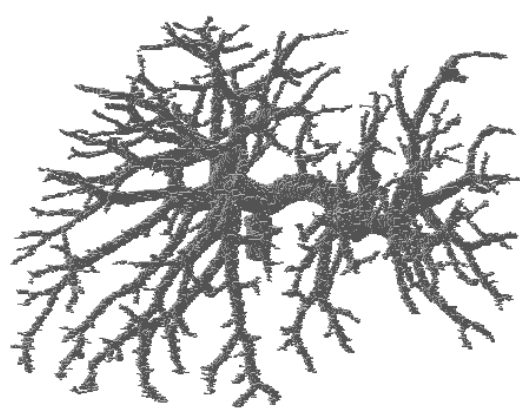
Because of the importance of the vessel segmentation for segment approximation, a phantom data set was generated based on the pruned version of the portal vein corrosion cast tree and the reconstructed liver mask. Liver tissue is modeled homogeneously in axial images and shows an exponential gray-value transition from 106 HU (Hounsfield Units) to 156 HU* in z direction, to model the ongoing contrast enrichment during the portal phase scan. Vessel intensities are ranging from 169 HU to 183 HU, with lower values corresponding to smaller vessels. Voxel and volume sizes were not altered compared to the original corrosion cast scan. CT “realistic” noise is modeled by Radon transforming each axial slice of the volume, adding Gaussian noise to the transformation, and by applying an inverse Radon transformation to obtain a noisy axial slice. For both transforms, angles between 0 and 179 degrees, with 1 degree increments, were used. The induced noise has a variance of 106 HU^2 inside the liver mask. As an example, a coronal slice of a phantom data set is shown in Figure 2(b).

In addition to the phantom data, a routinely acquired liver CT data set (LightSpeed QX/i, GE Medical Systems) with a voxel size of $0.55 \times 0.55 \times 2 \text{ mm}^3$ and a volume size of $512 \times 512 \times 96$ voxels was used for comparing segmentation algorithms only. The CT data set shows a relatively high contrast between the portal vessels and liver tissue.

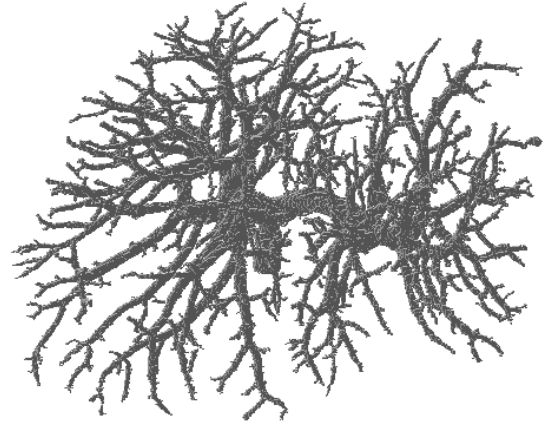
3.2. Quantitative Indices

Approximated liver volumes are compared to the reference approximation (Section 3.1) by reporting the relative volume errors in percent. For vessel segmentation analysis, missing vessels were detected by taking the reference segmentation (Section 3.1) in the form of a labeled volume and setting all voxels found by a segmentation algorithm to zero in the labeled volume. Remaining parts in the labeled volume correspond with undetected vessels and were individually marked by using a connected component labeling in a 26-neighborhood. To exclude responses in cases of under-segmented vessels, segmentation results were dilated by a spherical mask with a diameter of seven voxels. Afterwards, missing vessel parts were analyzed regarding their length L and radius R . L was calculated by evaluating the branch length via the Euclidean distance between skeleton voxels (Section

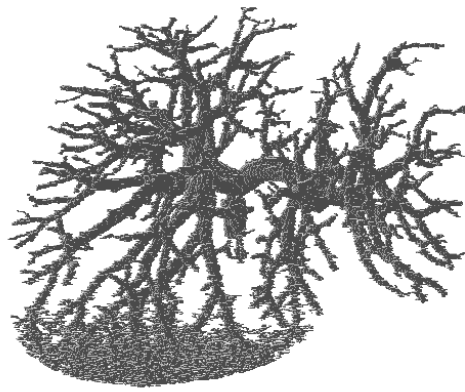
*All HU-values are reported without taking later added noise into account.



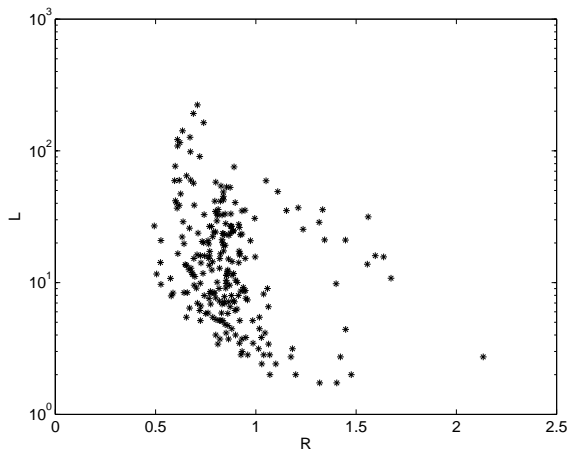
(a)



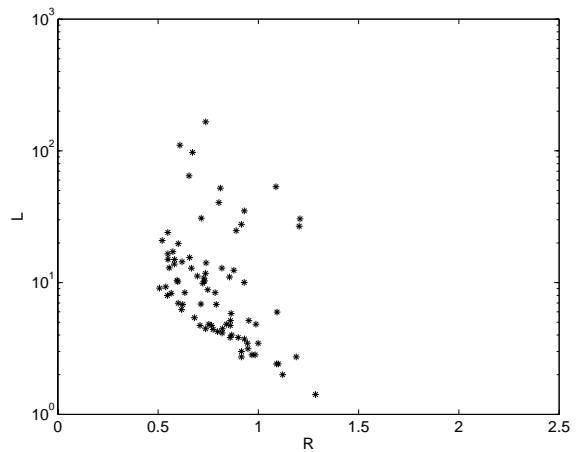
(b)



(c)



(d)



(e)

Figure 3. Portal vein segmentation results for the computer generated phantom data set. (a) Result of the region growing algorithm using an optimal selection of the threshold parameter (just before leakage). (b) Segmented vessel by the proposed vessel segmentation method. (c) Region growing algorithm with a non-optimal threshold selection. Plots of radius R versus vessel length L of vessels which failed to be segmented by the region growing method (d) and which failed using the proposed method (e). More details regarding R and L can be found in Section 3.2.

2.2), and R under the assumption of “cylindrical” vessels by evaluating $R = \sqrt{V_{branch}/L\pi}$, where V_{branch} is the volume of the missing vessel. Missing vessels with a voxel count lower than 50 were excluded from further analysis steps, since they were regarded as not significant enough. The errors are reported as mean \pm standard deviation.

4. RESULTS

The phantom data set was segmented by the proposed method with the following parameter settings: $T_{low} = 150$ HU, $T_{high} = 200$ HU, $\sigma = 0.8(1.5^n)$ voxel with $n = 1, \dots, 6$, $\gamma_{12} = 1.0$, $\gamma_{23} = 1.0$, $\alpha = 0.25$, $\beta = 0.01$, $T_1 = 50$ voxel, $T_2 = 4$ voxel, and $T_3 = 15$. For comparison, a region growing algorithm was applied to the same data set that was preprocessed with a Gaussian filter mask of size 5×5 and a sigma value of 1.5 applied to axial images. A 26-neighborhood connectedness was used for the growing process and only voxels with gray-values larger than the seed voxel gray value minus a threshold value were considered. The segmented vessel trees are shown in Figures 3(a) and 3(b), respectively. For the region growing result in Figure 3(b), an optimal threshold value was selected by just avoiding leakage. Figure 3(c) shows a result of the same algorithm with a different parameter setting clearly leaking into the simulated liver tissue. Plots of the radius R versus the vessel length L of missing vessels can be found in Figures 3(d) and 3(e) for the region growing algorithm and the proposed method, respectively. Analysis of missing vessels yielded the following results for average length \bar{L} and average radius \bar{R} for the region grower: $\bar{L} = 22.8 \pm 29.7$ mm and $\bar{R} = 0.87 \pm 0.22$ mm. Results for the proposed method were as follows: $\bar{L} = 16.2 \pm 25.2$ mm and $\bar{R} = 0.79 \pm 0.18$ mm. The number of missing vessels is 237 for the region growing method and 81 for the proposed method. For the vessel trees shown in Figures 3(a) and 3(b) the segment feeding vessels were identified manually by using the AR labeling tool (Section 2.3). All eight liver segments were then approximated by using the NNA method (see Fig. 4). The relative volume error of each segment compared to the reference approximation was calculated (Table 1). Regarding relative volume error, a mean absolute error over all eight segments was 6.03 ± 3.40 % for the region growing method and 1.95 ± 1.27 % for the proposed method.

Both segmentation methods were also applied to real CT data (see Section 3.1). Again, an “optimal” parameter setting was used for the region growing method. The proposed method was applied with the same parameter setting as for the phantom data set. Results can be seen in Figure 5. No analysis of missing vessels or relative approximation volume error calculation was performed, because of the lack of reference data.

Table 1. Relative volume errors for different portal vein segmentation methods using the NNA method on phantom data for liver segments one to eight.

Segment	1	2	3	4	5	6	7	8
Region growing	-12.3 %	7.7 %	4.9 %	-7.1 %	2.4 %	-3.7 %	7.9 %	2.2 %
Proposed method	-3.7 %	3.4 %	0.9 %	-1.7 %	1.2 %	-1.9 %	2.8 %	-0.1 %

5. DISCUSSION

The proposed vessel mining approach shows, that a larger percentage and generally smaller vessels can be segmented in the cases of the computer generated phantom data set and the real CT data, compared to a conventional region growing approach. Results on the phantom data set demonstrate that unidentified vessels were shorter and thinner. The relative volume error of the liver segment approximations based on segmented portal trees in phantom data indicate that the higher number of vessel branches segmented by the proposed vessel mining approach translates directly into a more accurate liver segment partitioning. In case of the phantom data, this was observed in all eight segments.

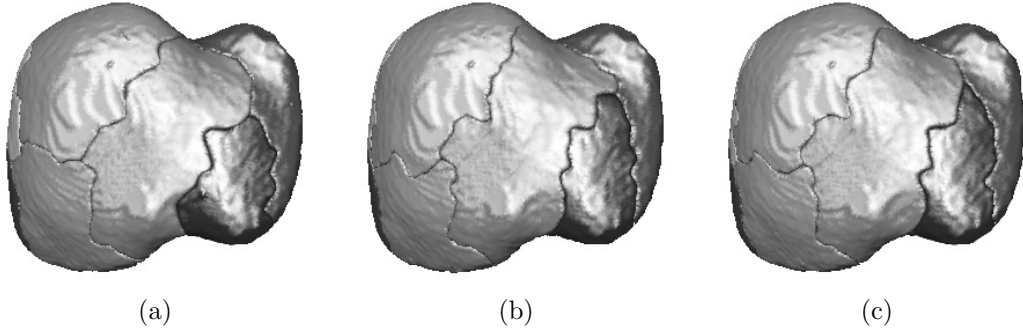


Figure 4. Comparison of approximated liver segments using the NNA method based on different vessel segmentation methods. (a) Approximation based on region growing vessel segmentation. (b) Reference segment approximation (see Section 3.1). (c) Segment approximation based on proposed vessel segmentation method.

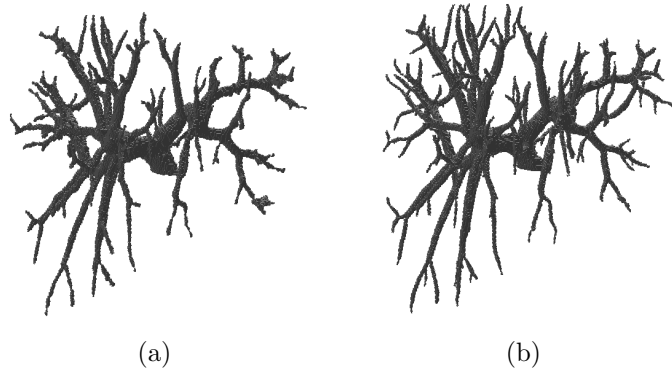


Figure 5. Vessel segmentation methods applied to a liver CT data set. (a) Region growing result and (b) result of the proposed method.

6. CONCLUSION

To facilitate segment-based liver tumor resection planning, a robust portal vein segmentation method was developed and validated in the context of liver segment approximation. The vessel segmentation method outperformed a conventional region growing approach with an optimal parameter setting both directly considering segmentation results as well as indirectly considering volume errors of approximated liver segments.

Taking the results of the relative volume errors of the approximated segments and comparing the complexity of the of the portal vessel tree of the segmented phantom data (Figs. 3(a) and 3(b)) with the one of the segmented real CT data (Fig. 5(a) and 5(b)) leads to the conclusion that a robust portal vein segmentation method is of paramount importance for liver segment approximation in routinely acquired CT data sets. Consequently, accurate vessel segmentation is a basis for precise preoperative planning of liver resections.

Future work will focus on advanced reconnection strategies and on even higher selectivity of the Hessian matrix based vessel enhancement step.

ACKNOWLEDGMENTS

This work was supported by the Austrian Science Foundation (FWF) under grant P14897-N04 and P17066-N04. We are grateful for the support of this work by Prof. Dr. Friedrich Anderhuber from the Institute of Anatomy at University Hospital Graz who provided a portal vein corrosion cast.

REFERENCES

1. J. Scheele, "Anatomical and atypical liver resection," *Chirurg* **72**(2), pp. 113–124, 2001.
2. C. Couinaud, *Le Foie – Etudes anatomiques et chirurgicales*, Masson, Paris, 1957.
3. H. Strunk, G. Stuckmann, J. Textor, and W. Willinek, "Limitations and pitfalls of Couinaud's segmentation of the liver in transaxial Imaging," *European Radiology* **13**(11), pp. 2472–2482, 2003.
4. H. Borquain, A. Schenk, F. Link, B. Preim, G. Prause, and H.-O. Peitgen, "HepaVision2 - a software assistant for preoperative planning in living-related liver transplantation and oncologic liver surgery," in *Proceedings of the 16th International Congress of Computer Assisted Radiology and Surgery*, pp. 341–346, CARS, June 2002.
5. D. Högemann, G. Stamm, H. Shin, H. Schlitt, D. Selle, and H.-O. Peitgen, "Individuelle Planung leberchirurgischer Eingriffe an einem virtuellen Modell der Leber und ihrer Leitstrukturen," *Der Radiologe* **40**, pp. 267–273, 2000.
6. H.-P. Meinzer, M. Thorn, and C. Cardenas, "Computerized planning of liver surgery - an overview," *Computers & Graphics* **26**, pp. 569–576, August 2002.
7. G. Glombitza, W. Lamadé, A. Demiris, M. Göpfert, A. Mayer, M. Bahner, H.-P. Meinzer, G. Richter, T. Lehnert, and C. Herfarth, "Virtual planning of liver resections: Image processing, visualization and volumetric evaluation," *Int. Journal of Medical Informatics* **53**, pp. 225–237, 1999.
8. L. Soler, H. Delingette, G. Malandain, J. Montagnat, N. Ayache, C. Koehl, O. Dourthe, B. Malassagne, M. Smith, D. Mutter, and J. Marescaux, "Fully automatic anatomical, pathological, and functional segmentation from CT scans for hepatic surgery," *Computer Aided Surgery* **6**(3), pp. 131–142, 2001.
9. L. Soler, H. Delingette, G. Malandain, J. Montagnat, N. Ayache, J.-M. Clément, C. Koehl, O. Dourthe, D. Mutter, and J. Marescaux, "A fully automatic anatomical, pathological and functional segmentation from CT-scans for hepatic surgery," in *Medical Imaging 2000, SPIE proceedings*, pp. 246–255, SPIE, (San Diego), Feb. 2000.
10. A. Bornik, R. Beichel, B. Reitinger, G. Gotschuli, E. Sorantin, F. Leberl, and M. Sonka, "Computer aided liver surgery planning: An augmented reality approach," in *SPIE Medical Imaging 2003: Visualization, Image-Guided Procedures and Display*, February 2003.
11. A. Bornik, R. Beichel, B. Reitinger, G. Gotschuli, E. Sorantin, F. Leberl, and M. Sonka, "Computer aided liver surgery planning based on augmented reality techniques," in *Bildverarbeitung für die Medizin 2003*, T. Wittenberg, P. Hastreiter, U. Hoppe, H. Handels, A. Horsch, and H.-P. Meinzer, eds., pp. 249–253, Springer, 2003. ISBN 30540-00619-2.
12. J. Fasel, D. Selle, C. Evertsz, F. Terrier, H. Peitgen, and P. Gailloud, "Segmental anatomy of the liver: poor correlation with CT," *Radiology* **206**(1), pp. 151–156, 1998.
13. L. Fischer, C. Cardenas, M. Thorn, A. Benner, L. Grenacher, M. Vetter, T. Lehnert, E. Klar, H.-P. Meinzer, and W. Lamade, "Limits of Couinaud's liver segment classification: a quantitative computer-based three-dimensional analysis," *J Comput Assist Tomogr* **26**(6), pp. 962–967, 2002.
14. D. Selle, B. Preim, A. Schenk, and H.-O. Peitgen, "Analysis of vasculature for liver surgical planning," *IEEE Transactions on Medical Imaging* **21**(11), pp. 1344–1357, 2002.
15. Y. Sato, S. Nakajima, H. Atsumi, T. Koller, G. Gerig, S. Yoshida, and R. Kikinis, "3D Multi-Scale Line Filter for Segmentation and Visualization of Curvilinear Structures in Medical Images," in *First Joint Conference of CVRMed II and MRCAS III (CVRMed-MRCAS'97)*, *Lecture Notes in Computer Science* **1205**, pp. 213–222, Springer-Verlag, (Berlin), 1997.
16. C. Lorenz, I. C. Carlsen, T. M. Buzug, C. Fassnacht, and J. Weese, "Multi-scale line segmentation with automatic estimation of width, contrast and tangential direction in 2D and 3D medical images," in *First Joint Conference of CVRMed II and MRCAS III (CVRMed-MRCAS'97)*, *Lecture Notes in Computer Science* **1205**, pp. 233–242, Springer-Verlag, (Berlin), 1997.
17. Y. Sato, S. Nakajima, N. Shiraga, H. Atsumi, S. Yoshida, T. Koller, G. Gerig, and R. Kikinis, "Three-Dimensional Multi-Scale Line Filter for Segmentation and Visualization of Curvilinear Structures in Medical Images," *Medical Image Analysis* **2**(2), pp. 143–168, 1998.

18. A. Frangi, W. Niessen, K. Vincken, and M. Viergever, "Multiscale vessel enhancement filtering," in *Image Computing and Computer-Assisted Intervention - MICCAI'98*, W. Wells, A. Colchester, and S. Delp, eds., *Lecture Notes in Computer Science* **1496**, pp. 130–137, Springer Verlag, 1998.
19. A. Frangi, W. Niessen, R. Hoogeveen, T. van Walsum, and M. Viergever, "Model-based Quantitation of 3D Magnetic Resonance Angiographic Images," *IEEE Trans on Medical Imaging* **18**(10), pp. 946–956, 1999.
20. M. E. Martinez-Perez, A. D. Hughes, A. V. Stanton, S. A. Thom, A. A. Bharath, and K. H. Parker, "Retinal blood vessel segmentation by means of scale-space analysis and region growing," in *Medical Image Computing and Computer-Assisted Intervention (MICCAI'99)*, pp. 90–97, 1999.
21. W. J. Niessen, C. M. van Bommel, A. F. Frangi, M. J. A. Siers, and O. Wink, "Model-based segmentation of cardiac and vascular images," in *IEEE International Symposium on Biomedical Imaging*, M. Unser and Z.-P. Liang, eds., pp. 22–25, (Washington DC, USA), 2002.
22. O. Wink, A. Frangi, B. Verdonck, M. Viergever, and W. Niessen, "3D MRA Coronary Axis Determination using a Minimum Cost Path Approach," *Magnetic Resonance in Medicine* **47**(1), pp. 1169–1175, 2002.
23. S. Aylward and E. Bullitt, "Initialization, noise, singularities, and scale in height ridge traversal for tubular object centerline extraction," *IEEE Transactions on Medical Imaging* **21**(2), pp. 61–75, 2002.
24. C. van Bommel, O. Wink, B. Verdonck, M. Viergever, and W. Niessen, "Blood pool contrast-enhanced MRA: improved arterial visualization in the steady state," *IEEE Transactions on Medical Imaging* **22**(5), pp. 645–652, 2003.
25. Q. Lin, *Enhancement, Extraction, and Visualization of 3D Volume Data*. PhD thesis, Department of Electrical Engineering, Linköping University, SE-581 83 Linköping, Sweden, April 2003.
26. O. Wink, W. Niessen, and M. Viergever, "Multiscale vessel tracking," *IEEE Transactions on Medical Imaging* **23**(1), pp. 130–133, 2004.
27. M. Näf, G. Székely, R. Kikinis, M. Shenton, and G. Kübler, "3D Voronoi skeletons and their usage for the characterization and recognition of 3D organ shape," *Computer Vision, Graphics, and Image Processing* **66**(2), pp. 147–161, 1997.
28. K. Palágyi, J. Tschirren, and M. Sonka, "Quantitative analysis of three-dimensional tubular tree structures," in *Medical Imaging 2003: Image Processing*, **5032**, pp. 277–287, SPIE, 2003.
29. K. Palágyi, J. Tschirren, and M. Sonka, "Quantitative analysis of intrathoracic airway trees: methods and validation," in *Information Processing in Medical Imaging, IPMI 2003, Lecture Notes in Computer Science* **2732**, pp. 222–233, Springer, 2003.
30. H.-O. Peitgen, D. Selle, J. Fasel, K. Klose, H. Jürgens, and C. Evertsz, "Mathematik, Komplexe Systeme, Medizin: Von der Potentialtheorie zu neuen radiologischen Werkzeugen," in *Visualisierung in Mathematik, Technik und Kunst. Grundlagen und Anwendungen*, A. Dress and G. Jäger, eds., pp. 91–107, Vieweg und Sohn Verlagsgesellschaft, 1999.
31. N. Otsu, "A threshold selection method from gray level histograms," *IEEE Trans. Systems, Man and Cybernetics* **9**, pp. 62–66, Mar. 1979.
32. T. Kong and A. Rosenfeld, "Digital topology: Introduction and survey," *Computer Vision, Graphics, and Image Processing* **48**, pp. 357–393, 1989.
33. B. Reitinger, A. Bornik, R. Beichel, G. Werkgartner, and E. Sorantin, "Tools for augmented reality-based liver resection planning," in *Medical Imaging 2004: Visualization, Image-Guided Procedures, and Display*, J. Robert L. Galloway, ed., **5367**, SPIE, 2004. To appear.
34. H. Delingette, *Modélisation, Déformation et Reconnaissance d'objets tridimensionnels à l'aide de maillages simplexes*. Thèse de sciences, Ecole Centrale de Paris, July 1994.
35. B. Reitinger, A. Bornik, and R. Beichel, "Efficient volume measurement using voxelization," in *Proc. of the Spring Conference on Computer Graphics 2003*, K. Joy and L. Szirmay-Kalos, eds., pp. 57–64, Comenius University, Bratislava, (Budmerice), April 2003.